Article

Characterization of SARS-CoV-2 Omicron BA.4 and BA.5 isolates in rodents

https://doi.org/10.1038/s41586-022-05482-7

Received: 3 July 2022

Accepted: 25 October 2022

Published online: 2 November 2022

Check for updates

Ryuta Uraki[1,2,12], Peter J. Halfmann[3,12], Shun Iida[4,12], Seiya Yamayoshi[1,2,12], Yuri Furusawa[1,2], Maki Kiso[1], Mutsumi Ito[1], Kiyoko Iwatsuki-Horimoto[1], Sohtaro Mine[4], Makoto Kuroda[3], Tadashi Maemura[3], Yuko Sakai-Tagawa[1], Hiroshi Ueki[1,2], Rong Li[5], Yanan Liu[5], Deanna Larson[5], Shuetsu Fukushi[6], Shinji Watanabe[7], Ken Maeda[8], Andrew Pekosz[9], Ahmed Kandeil[10,11], Richard J. Webby[10], Zhongde Wang[5], Masaki Imai[1,2]✉, Tadaki Suzuki[4]✉ & Yoshihiro Kawaoka[1,2,3]✉

The BA.2 sublineage of the SARS-CoV-2 Omicron variant has become dominant in most countries around the world; however, the prevalence of BA.4 and BA.5 is increasing rapidly in several regions. BA.2 is less pathogenic in animal models than previously circulating variants of concern[1–4]. Compared with BA.2, however, BA.4 and BA.5 possess additional substitutions in the spike protein, which play a key role in viral entry, raising concerns that the replication capacity and pathogenicity of BA.4 and BA.5 are higher than those of BA.2. Here we have evaluated the replicative ability and pathogenicity of BA.4 and BA.5 isolates in wild-type Syrian hamsters, human ACE2 (hACE2) transgenic hamsters and hACE2 transgenic mice. We have observed no obvious differences among BA.2, BA.4 and BA.5 isolates in growth ability or pathogenicity in rodent models, and less pathogenicity compared to a previously circulating Delta (B.1.617.2 lineage) isolate. In addition, in vivo competition experiments revealed that BA.5 outcompeted BA.2 in hamsters, whereas BA.4 and BA.2 exhibited similar fitness. These findings suggest that BA.4 and BA.5 clinical isolates have similar pathogenicity to BA.2 in rodents and that BA.5 possesses viral fitness superior to that of BA.2.

The Omicron (B.1.1.529 lineage) variant of severe acute respiratory syndrome coronavirus 2 (SARS-CoV-2), which is responsible for coronavirus disease 2019 (COVID-19) (WHO dashboard https://covid19.who.int), has spread rapidly worldwide and has become the dominant variant circulating globally. Omicron variants have been classified into at least five different sublineages: BA.1, BA.2, BA.3, BA.4 and BA.5. As of June 2022, BA.2 has become the most prevalent sublineage, replacing the previously dominant BA.1 sublineage, in most countries around the world; however, BA.4 and BA.5 were predominant in South Africa and Botswana and Portugal (https://covariants.org/per-variant). In addition, the prevalence of BA.5 is increasing rapidly in many European countries. Preliminary data suggest that BA.4 and BA.5 may be more transmissible than the other Omicron variants[5].

Recently, we and others have demonstrated that both the BA.1 and BA.2 sublineages are less pathogenic in animal models than previously circulating variants of concern, consistent with clinical data in humans[1–4,6–8]. Compared with BA.2, both BA.4 and BA.5 possess three additional changes (69–70del, L452R and F486V) and one reversion mutation (R493Q) in their spike (S) proteins, which play a pivotal role in viral entry. The BA.1 subvariants also do not have the two additional mutations, L452R and F486V. Previous studies have shown that the L452R mutation increases the fusogenicity and infectivity of SARS-CoV-2 variants including Omicron[9–11]. However, the biological properties of BA.4 and BA.5 isolates are unknown. Here, we assessed the replicative capacity and pathogenicity of BA.4 and BA.5 isolated from COVID-19 patients in established COVID-19 animal models.

BA.4 and BA.5 infection in hamsters

To characterize the BA.4 and BA.5 variants in vivo, we amplified the following BA.4 and BA.5 clinical isolates: hCoV-19/USA/MD/HP30386/2022 (BA.4: HP30386) and SARS-CoV-2/human/USA/COR-22-063113/2022 (BA.5: COR-22-063113), propagated in VeroE6-TMPRSS2-T2A-ACE2 cells; and hCoV-19/Japan/TY41-703/2022 (BA.4: TY41-703), hCoV-19/Japan/TY41-702/2022 (BA.5: TY41-702) and hCoV-19/Japan/TY41-704/2022 (BA.5: TY41-704), propagated in VeroE6/TMPRSS2 cells. We confirmed

[1]Division of Virology, Institute of Medical Science, University of Tokyo, Tokyo, Japan. [2]The Research Center for Global Viral Diseases, National Center for Global Health and Medicine Research Institute, Tokyo, Japan. [3]Influenza Research Institute, Department of Pathobiological Sciences, School of Veterinary Medicine, University of Wisconsin-Madison, Madison, WI, USA. [4]Department of Pathology, National Institute of Infectious Diseases, Tokyo, Japan. [5]Department of Animal, Dairy, and Veterinary Sciences, College of Agriculture and Applied Sciences, Utah State University, Logan, UT, USA. [6]Department of Virology 1, National Institute of Infectious Diseases, Tokyo, Japan. [7]Center for Influenza and Respiratory Virus Research, National Institute of Infectious Diseases, Tokyo, Japan. [8]Department of Veterinary Science, National Institute of Infectious Diseases, Tokyo, Japan. [9]W. Harry Feinstone Department of Molecular Microbiology and Immunology, The Johns Hopkins Bloomberg School of Public Health, Baltimore, MD, USA. [10]Department of Infectious Diseases, St Jude Children's Research Hospital, Memphis, TN, USA. [11]Center of Scientific Excellence for Influenza Viruses, National Research Centre, Giza, Egypt. [12]These authors contributed equally: Ryuta Uraki, Peter J. Halfmann, Shun Iida, Seiya Yamayoshi.
✉e-mail: mimai@ims.u-tokyo.ac.jp; tksuzuki@niid.go.jp; yoshihiro.kawaoka@wisc.edu

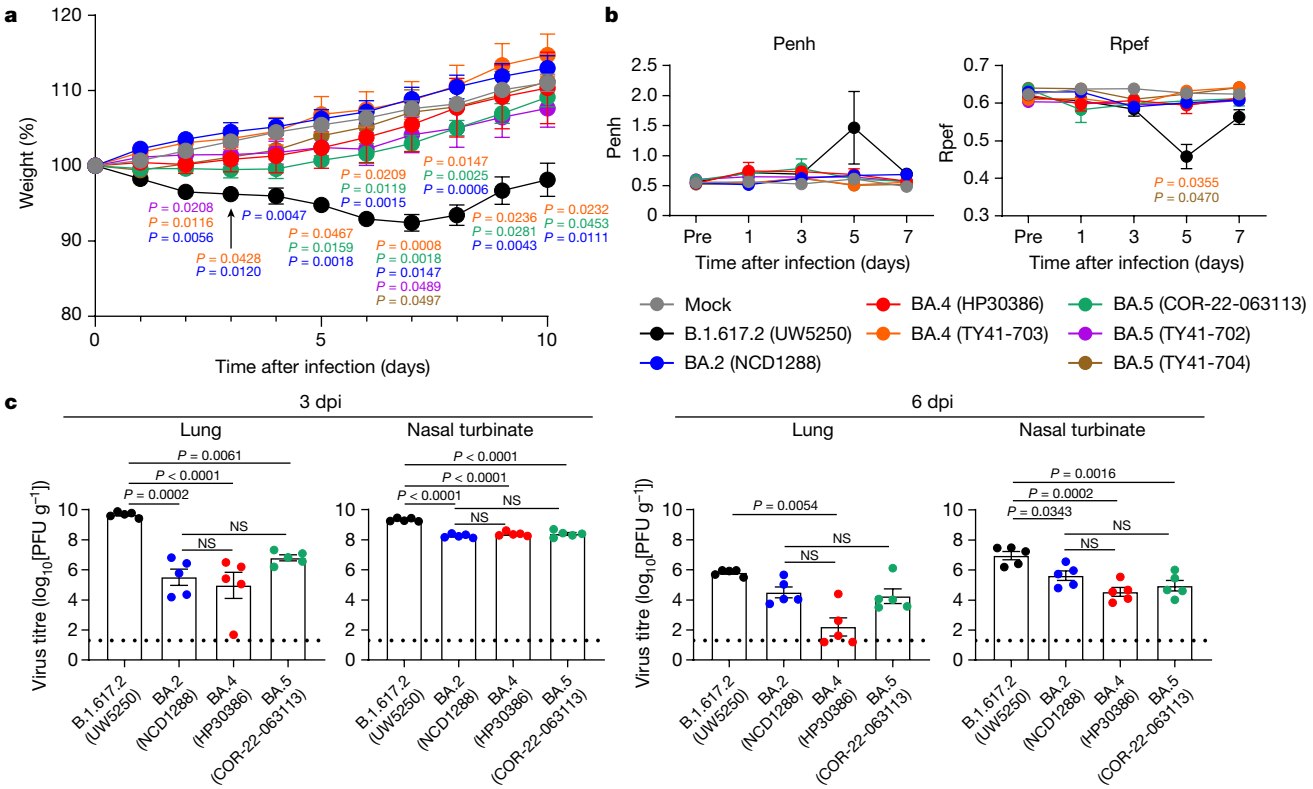

Fig. 1 | The replication and pathogenicity of BA.2, BA.4 and BA.5 isolates in wild-type hamsters. a,**b**, Wild-type Syrian hamsters were intranasally inoculated with 10^5 PFU in 30 µl of BA.2 (NCD1288), BA.4 (HP30386 or TY41-703), BA.5 (COR-22-063113, TY41-702 or TY41-704), B.1.617.2 (UW5250) or phosphate-buffered saline (mock). **a**, Body weights of virus-infected ($n = 5$) and mock-infected hamsters ($n = 7$) were monitored daily for ten days. **b**, Pulmonary function analyses in virus-infected ($n = 5$) and mock-infected hamsters ($n = 7$). Penh and Rpef were measured by using whole-body plethysmography. Data are presented as the mean ± standard error of the mean (s.e.m.). Data were analysed by using a two-way analysis of variance (ANOVA) followed by Tukey's multiple comparisons. **c**, Virus replication in infected Syrian hamsters. Hamsters ($n = 10$) were intranasally inoculated with 10^5 PFU in 30 µl of BA.2 (NCD1288), BA.4 (HP30386), BA.5 (COR-22-063113) or B.1.617.2 (UW5250) and euthanized at 3 and 6 dpi for virus titration ($n = 5$ day^{-1}). Virus titres in the nasal turbinates and lungs were determined by performing plaque assays with VeroE6-TMPRSS2-T2A-ACE2 cells. Vertical bars show the mean ± s.e.m. Points indicate data from individual hamsters. The lower limit of detection is indicated by the horizontal dashed line. Data were analysed by using a one-way ANOVA with Tukey's multiple comparisons test (titre in the lungs at 3 dpi and nasal turbinates at 3 and 6 dpi) or the Kruskal–Wallis test followed by Dunn's test (titre in the lungs at 6 dpi). *P* values of less than 0.05 were considered statistically significant. Data are from one experiment. NS, not significant.

that all five isolates contained the five additional amino acid changes (that is, 69–70del, L452R, F486V and reversion mutation R493Q), compared to a BA.2 isolate (hCoV-19/Japan/UT-NCD1288-2N/2022; NCD1288) (Extended Data Table 1). However, the two BA.4 isolates (HP30386 and TY41-703) had a V3G substitution in the signal peptide region of S, in addition to the five mutations. One BA.5 isolate (COR-22-063113) encoded a T76I substitution in the N-terminal domain (NTD), and another BA.5 isolate (TY41-704) possessed a mixed viral population encoding either R or W at position 682.

We first evaluated the pathogenicity of the two BA.4 and three BA.5 isolates in wild-type Syrian hamsters, a well-established small animal model[12–14] for the study of COVID-19. Syrian hamsters were intranasally inoculated with 10^5 plaque-forming units (PFU) of BA.4 (HP30386 or TY41-703) or BA.5 (COR-22-063113, TY41-702 or TY41-704). For comparison, additional hamsters were infected with 10^5 PFU of BA.2 (NCD1288) or B.1.617.2 (hCoV-19/USA/WI-UW-5250/2021: UW5250). Intranasal infection with B.1.617.2 resulted in remarkable body weight loss by seven days post-infection (dpi) (−7.6%) (Fig. 1a) consistent with our previous observations[1]. By contrast, all or most of the animals infected with the BA.2, BA.4 or BA.5 isolates gained weight over the ten-day experiment, similar to the mock-infected animals. Compared with the B.1.617.2-infected group, significant differences in weight changes were observed in the BA.4 (TY41-703)- and BA.5 (COR-22-063113, TY41-702 or TY41-704)-infected groups at some timepoints, but not the BA.4 (HP30386)-infected group. No significant differences in weight changes were found among the BA.2-, BA.4- and BA.5-infected groups. We also assessed pulmonary function in the infected hamsters by measuring Penh and Rpef, which are surrogate markers for bronchoconstriction and airway obstruction, respectively, by using a whole-body plethysmography system (Fig. 1b). Infection with the BA.2 (NCD1288), BA.4 (HP30386 or TY41-703) or BA.5 (COR-22-063113, TY41-702 or TY41-704) isolates did not cause substantial changes in either Penh or Rpef compared with the mock-infected group at any timepoint after infection. By contrast, infection with B.1.617.2 caused notable changes in Penh and Rpef at 5 dpi.

We next assessed levels of infection in the respiratory tract of wild-type hamsters infected with 10^5 PFU of BA.4 (HP30386), BA.5 (COR-22-063113), BA.2 (NCD1288) or B.1.617.2 (UW5250) (Fig. 1c). BA.4, BA.5 and BA.2 replicated in the lungs and nasal turbinates of the infected animals with no significant differences in viral titre at both timepoints examined. However, at 3 dpi, the virus titres were significantly lower in the respiratory tract of animals infected with BA.4 or BA.5, compared with animals infected with B.1.617.2 (mean differences in viral titre = 4.7 and 2.9 $\log_{10}$(PFU g^{-1}) and 0.95 and 0.94 $\log_{10}$(PFU g^{-1}) for the viral titre in the lungs and nasal turbinates, respectively). At 6 dpi, the virus titres in the lungs and nasal turbinates of the BA.4- or BA.5-infected group were also lower than those in the B.1.617.2-infected group (mean differences in viral titre = 1.3–3.6 $\log_{10}$ (PFU g^{-1}) and 1.3–2.4 $\log_{10}$ (PFU g^{-1}) in the lungs and nasal turbinates, respectively), although the differences in the lungs were not statistically significant between the BA.5- and

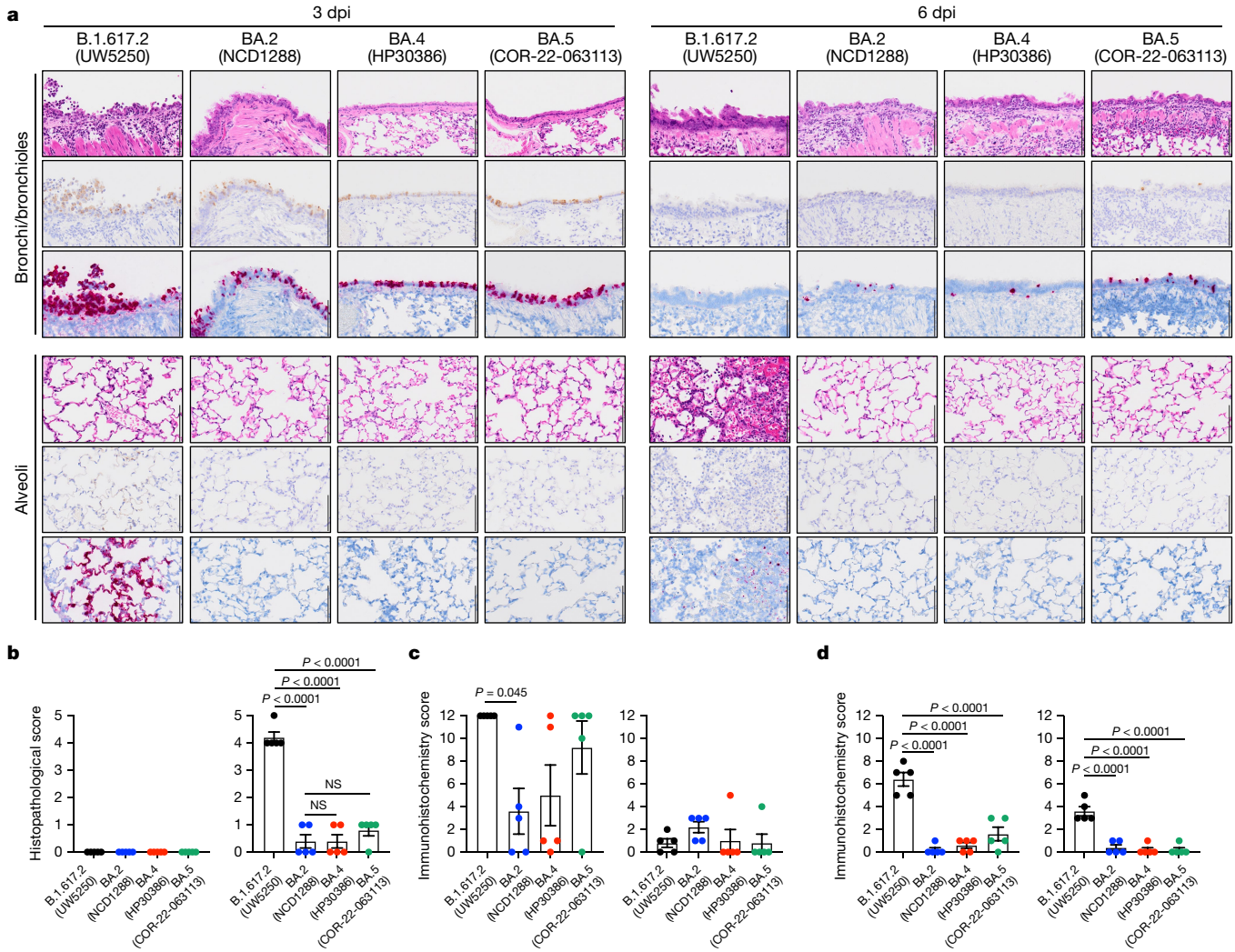

Fig. 2 | Histopathological findings in hamsters inoculated with SARS-CoV-2 Omicron sublineage viruses. Wild-type Syrian hamsters ($n = 5$, each per group) were inoculated with 10^5 PFU of BA.2 (NCD1288), BA.4 (HP30386), BA.5 (COR-22-063113) or B.1.617.2 (UW5250) viruses and euthanized at 3 and 6 dpi for histopathological examinations. Representative images of the bronchi/bronchioles and alveoli are shown. Upper rows, haematoxylin and eosin (H&E) staining. Middle rows, immunohistochemistry that detects the SARS-CoV-2 nucleocapsid protein. Lower rows, in situ hybridization targeting the nucleocapsid gene of SARS-CoV-2. Scale bars, 100 µm. **b**, Histopathological scores of inflammation in the alveoli. The scores were determined based on the percentage of alveolar inflammation in a given area of a pulmonary section collected from each animal in each group by using the following scoring system: 0, no inflammation; 1, affected area (≤1%); 2, affected area (>1%, ≤10%); 3, affected area (>10%, ≤50%); 4, affected area (>50%). An additional point was added when pulmonary oedema and/or alveolar haemorrhage was observed. Therefore, the scores for individual animals ranged from 0 to 5. **c**,**d**, Immunohistochemistry scores of bronchial/bronchiolar regions (**c**) and alveolar regions (**d**). The scores were determined based on the percentage of viral antigen-positive cells, detected by immunohistochemistry, in a high-power field by using the following scoring system: 0, no positive cells; 1, positive cells (≤10%); 2, positive cells (>10%, ≤25%); 3, positive cells (>25%, ≤50%); 4, positive cells (>50%). Immunohistochemistry scores for each animal were calculated for bronchial/bronchiolar and alveolar regions, respectively, as a total score for the three high-power fields with the highest positivity rate on the section; the scores for individual animals ranged from 0 to 12. Vertical bars show the mean ± s.e.m. Points indicate data from individual hamsters. Data were analysed by using a one-way ANOVA with Tukey's multiple comparisons test. *P* values of less than 0.05 were considered statistically significant. Data are from one experiment.

B.1.617.2-infected groups. These results demonstrate that the replicative abilities of BA.4 and BA.5 are similar to those of BA.2, and are attenuated compared with those of B.1.617.2.

Histopathology in infected hamsters

Syrian hamsters inoculated with BA.2 (NCD1288), BA.4 (HP30386), BA.5 (COR-22-063113) or B.1.617.2 (UW5250) were euthanized at 3 and 6 dpi, respectively, for histopathological analysis of the airways and lungs. In animals inoculated with any of the Omicron sublineage viruses, no obvious inflammation was observed in the peripheral airways or alveolar region at 3 dpi (Fig. 2a). At 6 dpi, infiltration of inflammatory cells (that is, mononuclear cells and neutrophils) was observed with these Omicron viruses in the peribronchial and peribronchiolar regions (Fig. 2a). Although small foci of inflammatory cell infiltration into the alveolar spaces were observed in some animals at 6 dpi, there was no evidence of pneumonia at either timepoint examined. By contrast, in B.1.617.2-inoculated animals, peribronchial/peribronchiolar inflammation was observed at 3 dpi, and massive infiltration of inflammatory cells with haemorrhage was prominent in the alveolar regions at 6 dpi (Fig. 2a). Histopathological scores of inflammation in the alveoli were comparable among the BA.2-, BA.4- and BA.5-inoculated groups at 6 dpi, whereas worse scores were obtained for the B.1.617.2-inoculated group at the same timepoint

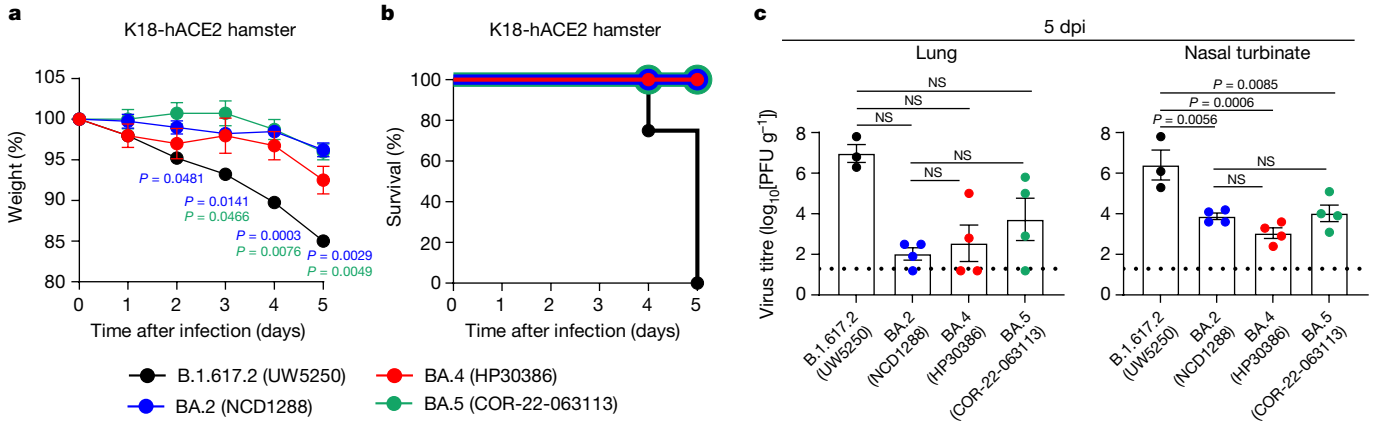

Fig. 3 | The replication and pathogenicity of BA.4 and BA.5 in hACE2-expressing hamsters. a–**c**, hACE2-expressing Syrian hamsters ($n = 4$) were intranasally inoculated with 10^5 PFU in 30 µl of BA.2 (NCD1288), BA.4 (HP30386), BA.5 (COR-22-063113) or B.1.617.2 (UW5250). Body weights (**a**) and survival (**b**) were monitored daily for 5 days. The data are presented as the mean percentages of the starting weight ± s.e.m. Body weight data were analysed by using a two-way ANOVA followed by Tukey's multiple comparisons. **c**, Infected hamsters were euthanized at 5 dpi for virus titration (BA.2, $n = 4$; BA.4, $n = 4$; BA.5, $n = 4$; B.1.617.2, $n = 3$). Virus titres in the nasal turbinates and lungs were determined by performing plaque assays with VeroE6-TMPRSS2-T2A-ACE2 cells. Vertical bars show the mean ± s.e.m. Points indicate data from individual hamsters. The lower limit of detection is indicated by the horizontal dashed line. Data were analysed by using a one-way ANOVA with Tukey's multiple comparisons test (titre in the nasal turbinates) or the Kruskal–Wallis test followed by Dunn's test (titre in the lungs). *P* values of less than 0.05 were considered statistically significant. Data are from one experiment.

(Fig. 2b). Immunohistochemistry revealed that the SARS-CoV-2 antigen was present on the bronchial/bronchiolar epithelium in the BA.2-, BA.4- or BA.5-inoculated animals at 3 dpi, with a clear decrease in antigen-positive cells over time (Fig. 2a,c). In the BA.2-, BA.4- or BA.5-inoculated animals, viral antigen was rarely detected in the alveolar regions at either timepoint examined (Fig. 2a,d); the distribution of viral RNA, determined by in situ hybridization, was similar for all three inoculated groups (Fig. 2a). By contrast, viral antigen and RNA were detected not only in the bronchial/bronchiolar regions but also in the alveolar regions at 3 dpi with the B.1.617.2 virus, both of which decreased over time (Fig. 2a,c,d).

In summary, there were no significant differences in the distribution of viral antigen/RNA-positive cells and extension of inflammation, which was limited to the peribronchial/peribronchiolar regions, among the BA.2-, BA.4- and BA.5-inoculated groups. These Omicron sublineage viruses also showed attenuated pathogenicity compared with the B.1.617.2 virus in the hamster model.

BA.4 and BA.5 infection in hACE2 rodents

We investigated the replication and pathogenicity of BA.4 and BA.5 by using a more susceptible rodent model, that is, hACE2-expressing transgenic hamsters[15]. B.1.617.2 infection in hACE2-expressing hamsters resulted in marked body weight loss by 5 dpi (Fig. 3a) and 100% mortality at 5 dpi (Fig. 3b). By contrast, the hamsters infected with BA.2 (NCD1288), BA.4 (HP30386) or BA.5 (COR-22-063113) exhibited less weight loss than those infected with B.1.617.2 (Fig. 3a) and all of them survived (Fig. 3b). At 5 dpi, BA.4, BA.5 and BA.2 replicated in the respiratory organs of the infected hamsters with no significant differences in viral titre. The viral titres in the nasal turbinates of hamsters infected with BA.4 or BA.5 were significantly lower than those of hamsters infected with B.1.617.2 (mean differences in viral titre = 2.5 and 3.3 $\log_{10}$ (PFU g^{-1}), respectively). The lung titres in the BA.4- or BA.5-infected groups were also substantially lower than those in the B.1.617.2-infected group (mean differences in viral titre = 4.4 and 3.2 $\log_{10}$ (PFU g^{-1}), respectively), although these differences did not reach statistical significance (Fig. 3c). These results indicate that the replicative abilities of BA.4 and BA.5 are similar to those of BA.2, and are attenuated compared with those of B.1.617.2 in hACE2-expressing hamsters, consistent with our findings in wild-type hamsters.

To further investigate the replication and pathogenicity of BA.4 and BA.5 isolates in vivo, we inoculated hACE2-expressing mice with BA.4 (HP30386) or BA.5 (COR-22-063113)[16,17]. Mice infected with B.1.617.2 experienced marked body weight loss (Extended Data Fig. 1a) and 100% mortality at 10 dpi (Extended Data Fig. 1b). By contrast, all mice infected with BA.2 (NCD1288), BA.4 (HP30386) or BA.5 (COR-22-063113) survived, consistent with our observations in hACE2-expressing hamsters. Although the animals infected with BA.2 showed substantial body weight loss, the animals infected with BA.4 or BA.5 gained body weight (Extended Data Fig. 1a,b). The lung titres of mice infected with BA.2, BA.4 or BA.5 were significantly lower than those of mice infected with B.1.617.2 at both 2 dpi and 5 dpi (Extended Data Fig. 1c). No marked differences in viral titre in the lungs were observed among BA.2-, BA.4- and BA.5-infected animals at either timepoint examined. We also histopathologically analysed the lungs of hACE2-expressing mice infected with BA.4 or BA.5. This evaluation revealed no obvious peribronchial/peribronchiolar inflammation in the lungs of virus-inoculated hACE2-expressing mice (Extended Data Fig. 1d). At 2 dpi, no obvious pneumonia was detected in any groups, although small foci of inflammatory cell infiltration in alveolar regions were observed in some animals (Extended Data Fig. 1d). Notably, at 5 dpi, mild and scattered inflammation in the alveoli was observed not only in the B.1.617.2-inoculated group, but also in all the Omicron sublineage virus-inoculated groups. The extent of inflammatory cell infiltration varied among the individual animals; however, there were no clear differences among the groups (Extended Data Fig. 1d).

Overall, our data show that the pathogenicity of BA.4 and BA.5 is similar to that of BA.2, and is attenuated compared to that of B.1.617.2 in hamsters and mice.

The replicative fitness of BA.4 and BA.5

To further compare the replicative fitness of BA.4 and BA.2, wild-type hamsters were intranasally inoculated with 2×10^5 PFU of a mixture (1:1) of BA.4 (HP30386) and BA.2 (NCD1288). At 2 and 4 dpi, the nasal turbinates and lungs of the infected hamsters were assessed by next-generation sequencing (NGS) to determine the proportion of each virus. At 2 dpi, the proportion of BA.4 in the lungs and nasal turbinates of all five infected animals had slightly increased compared to that in the inoculum, except for the lung sample from hamster number 2.

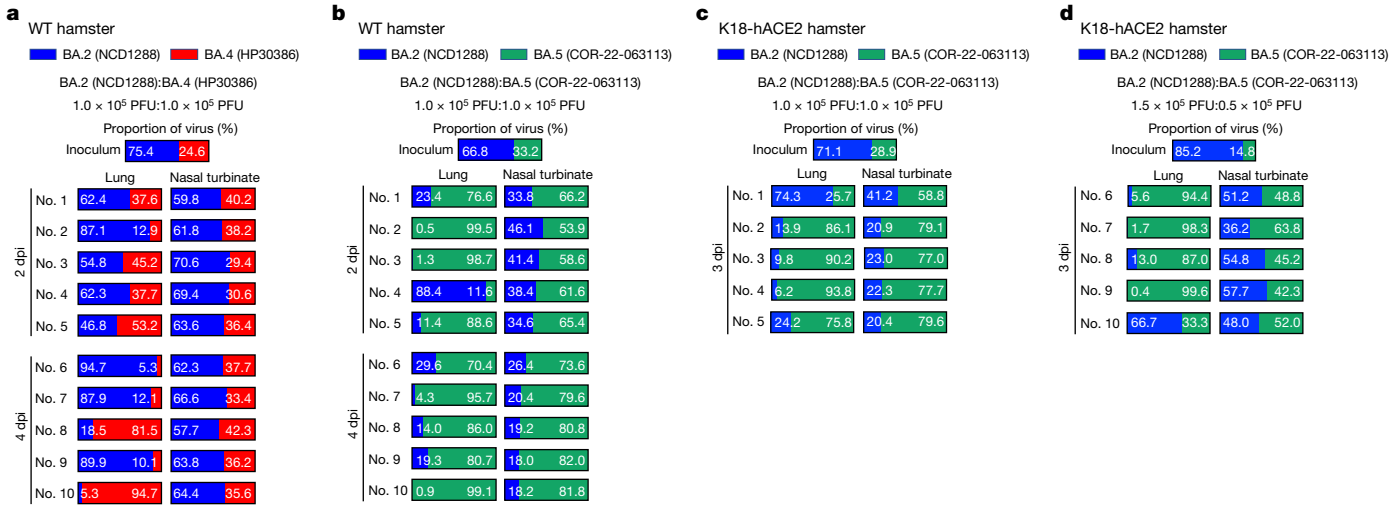

Fig. 4 | Replicative fitness of BA.4 and BA.5 compared with that of BA.2 in hamsters. a,**b**, BA.4 (HP30386) and BA.2 (NCD1288) (**a**) or BA.5 (COR-22-063113) and BA.2 (NCD1288) (**b**) were mixed at an equal ratio on the basis of their infectious titre, and the virus mixture (total 2×10^5 PFU in 60 µl) was intranasally inoculated into wild-type hamsters (total $n = 10$, $n = 5$ per day). Nasal turbinates and lungs were collected from the infected animals at 2 and 4 dpi and analysed by using NGS. The proportion of BA.2 and BA.4 or BA.2 and BA.5 was calculated from the five amino acid differences in the S gene between BA.2 and BA.4 or BA.2 and BA.5. **c**,**d**, BA.2 (NCD1288) and BA.5 (COR-22-063113) were mixed at a 1:1 (**c**) or 3:1 (**d**) ratio on the basis of their infectious titre, and the virus mixture (total 2×10^5 PFU in 60 µl) was intranasally inoculated into hACE2 transgenic hamsters ($n = 5$ per group). Nasal turbinates and lungs were collected from the infected animals at 3 dpi and analysed by using NGS. The proportion of BA.2 and BA.5 was calculated from the five amino acid differences in the S gene between the two viruses. Shown are the relative proportions of BA.2 and BA.4 (**a**) or BA.2 and BA.5 (**b**–**d**) in the infected animals. Data are from one experiment.

At dpi, the proportion of BA.4 had increased in the nasal turbinates of all five animals; however, the proportion in the lungs increased in only two of the five animals (Fig. 4a).

We next compared the viral fitness of BA.5 (COR-22-063113) and BA.2 (NCD1288) in wild-type hamsters (Fig. 4b). BA.5 was dominant in the nasal turbinates of all five infected animals at both 2 and 4 dpi. The lung samples also showed a greater proportion of BA.5 at both 2 and 4 dpi, except for the sample from animal number 4 at 2 dpi. A similar trend was observed for hACE2 hamsters inoculated with 2×10^5 PFU of a mixture of BA.2 (NCD1288) and BA.5 (TY41-702) at ratios of 1:1 or 3:1 (Fig. 4c,d). At 3 dpi, the proportion of BA.5 had increased in the nasal turbinates and lungs of all infected animals compared to that in each inoculum for either ratio, except for the lung sample from hamster number 1. Importantly, BA.5 became dominant in the lungs of eight (numbers 2, 3, 4, 5, 6, 7, 8 and 9) and in the nasal turbinates of seven (numbers 1, 2, 3, 4, 5, 7 and 10) of the ten animals (Fig. 4c,d).

Taken together, these results suggest that BA.5 may have greater replicative fitness than BA.2. In addition, our data suggest that the viral fitness of BA.4 is comparable or slightly greater than that of BA.2.

Discussion

Our data indicate that the sublineages BA.4 and BA.5 of SARS-CoV-2 Omicron variants are less pathogenic than B.1.617.2 in wild-type and hACE2-expressing hamsters, and hACE2-expressing mice. We observed that the clinical isolates of BA.4 and BA.5 were limited in their replication in the lungs of hamsters and mice, compared to a B.1.617.2 isolate (Fig. 1a–c). Moreover, histopathological examination revealed that viral antigens were rarely present in the alveoli of hamsters after infection with BA.4 or BA.5 (Fig. 2). Similar findings were obtained with clinical isolates of BA.1 and BA.2 (refs. [1,4,18]). These findings indicate that Omicron variants replicate less efficiently in the alveolar epithelial cells of rodents compared with B.1.617.2, which might contribute to the lower disease severity of Omicron variants seen in animal models.

We observed that BA.4 and BA.5 replicate efficiently in the nasal turbinates of hamsters, but not in the lungs (Fig. 1c), similar to BA.1 and BA.2 (refs. [1–4]). In human nasal epithelial cultures, Omicron and Delta variants have been reported to replicate with similar efficiency; however, in lower airway organoids and Calu-3 lung cells, Omicron variants replicate to lower titres than Delta variants[19]. Viral entry into host cells is mediated by the S protein. The S protein must be proteolytically activated by the human protein transmembrane protease serine 2 (TMPRSS2) at the cell surface or by cathepsin proteases within the endosomal cell compartment[20–23]. Interestingly, recent studies have suggested that the entry of Omicron variants is less dependent on TMPRSS2 activities but more sensitive to a cathepsin inhibitor compared with Delta variants[19,24]. This finding suggests that the TMPRSS2/cathepsin usage of the S protein may affect the viral replication efficiency in the lungs of humans and hamsters.

The BA.4 and BA.5 isolates, but not the BA.1 and BA.2 isolates, contain the L452R mutation in their S protein. A previous study demonstrated that the L452R mutation enhances the entry of a pseudovirus carrying the BA.1 S protein in K18-hACE2 transgenic mice[10]. Notably, a recent article (Kimura et al.[25]) reported that hamsters infected with 10^4 $TCID_{50}$ of a recombinant chimeric virus possessing the BA.4 or BA.5 S gene in the background of a BA.2 strain exhibited about 10% body weight loss and severe lung inflammation, whereas hamsters infected with parental recombinant BA.2 virus gained weight and experienced less inflammation in the lungs, suggesting that the S sequence differences between BA.2 and BA.4 or BA.5 are responsible for the difference in pathogenicity between these chimeric viruses; on the basis of these data, Kimura et al. concluded that BA.4 and BA.5 are more pathogenic than BA.2. However, in viruses isolated from patients, the genomes of BA.2, BA.4 and BA.5 differ at locations other than the S gene. Of the isolates we tested, the S protein sequence of the BA.5 isolate (TY41-702) was identical to that of the recombinant chimeric virus these authors tested (Extended Data Table 1). Infection with this BA.5 isolate did not cause substantial changes in either body weight or lung function in hamsters compared with the BA.2-infected group (Fig. 1a,b). Therefore,

differences at locations other than the S gene could offset differences in the pathogenic potential of the S gene.

We note several limitations in this study. (1) In hACE2 transgenic animals, we characterized one strain of BA.4 (that is, HP30386) and one strain of BA.5 (that is, COR-22-063113). Therefore, additional studies may be required to determine whether other BA.4 and/or BA.5 strains exhibit similar replication and pathogenicity to the strains tested. (2) Our study was conducted in healthy young animals; however, individuals aged 65 years and above and people with underlying medical conditions are at increased risk of severe COVID-19. Therefore, it remains unclear whether our data reflect the clinical outcomes in high-risk groups for COVID-19. (3) Our study was also performed in immunologically naive animals; however, many people have already acquired SARS-CoV-2-specific immunity through natural infection and/or vaccination. Therefore, it remains uncertain whether our data reflect the clinical outcome in patients with immunity to SARS-CoV-2. Recent preprint papers have reported that the severity of BA.5 in humans was similar to that of BA.1 or BA.2, consistent with our data[26–28]; however, more clinical data from patients infected with BA.4 or BA.5 are needed to corroborate the findings in the rodent models.

In summary, our data suggest that the sublineages BA.4 and BA.5 of SARS-CoV-2 Omicron variants have similar pathogenicity to that of the BA.2 sublineage in rodent models. Our results highlight the importance of evaluating viral replication and pathogenesis by using clinical isolates.

Online content

Any methods, additional references, Nature Portfolio reporting summaries, source data, extended data, supplementary information, acknowledgements, peer review information; details of author contributions and competing interests; and statements of data and code availability are available at https://doi.org/10.1038/s41586-022-05482-7.

1. Halfmann, P. J. et al. SARS-CoV-2 Omicron virus causes attenuated disease in mice and hamsters. *Nature* **603**, 687–692 (2022).
2. Shuai, H. et al. Attenuated replication and pathogenicity of SARS-CoV-2 B.1.1.529 Omicron. *Nature* **603**, 693–699 (2022).
3. Suzuki, R. et al. Attenuated fusogenicity and pathogenicity of SARS-CoV-2 Omicron variant. *Nature* **603**, 700–705 (2022).
4. Uraki, R. et al. Characterization and antiviral susceptibility of SARS-CoV-2 Omicron/BA.2. *Nature* **607**, 119–127 (2022).
5. Tegally, H. et al. Emergence of SARS-CoV-2 Omicron lineages BA.4 and BA.5 in South Africa. *Nat. Med.* https://doi.org/10.1038/s41591-022-01911-2 (2022).
6. Lewnard, J. A. et al. Clinical outcomes associated with SARS-CoV-2 Omicron (B.1.1.529) variant and BA.1/BA.1.1 or BA.2 subvariant infection in southern California. *Nat. Med.* **28**, 1933–1943 (2022).
7. Wolter, N. et al. Early assessment of the clinical severity of the SARS-CoV-2 Omicron variant in South Africa: a data linkage study. *Lancet* **399**, 437–446 (2022).
8. Ulloa, A. C., Buchan, S. A., Daneman, N. & Brown, K. A. Estimates of SARS-CoV-2 Omicron variant severity in Ontario, Canada. *JAMA* **327**, 1286–1288 (2022).
9. Motozono, C. et al. SARS-CoV-2 spike L452R variant evades cellular immunity and increases infectivity. *Cell Host Microbe* **29**, 1124–1136.e11 (2021).
10. Zhang, Y. et al. SARS-CoV-2 spike L452R mutation increases Omicron variant fusogenicity and infectivity as well as host glycolysis. *Signal Transduct. Target Ther.* **7**, 76 (2022).
11. Deng, X. et al. Transmission, infectivity, and neutralization of a spike L452R SARS-CoV-2 variant. *Cell* **184**, 3426–3437.e38 (2021).
12. Imai, M. et al. Syrian hamsters as a small animal model for SARS-CoV-2 infection and countermeasure development. *Proc. Natl Acad. Sci. USA* **117**, 16587–16595 (2020).
13. Sia, S. F. et al. Pathogenesis and transmission of SARS-CoV-2 in golden hamsters. *Nature* **583**, 834–838 (2020).
14. Chan, J. F. et al. Simulation of the clinical and pathological manifestations of coronavirus disease 2019 (COVID-19) in a golden Syrian hamster model: implications for disease pathogenesis and transmissibility. *Clin. Infect. Dis.* **71**, 2428–2446 (2020).
15. Gilliland, T. et al. Protection of human ACE2 transgenic Syrian hamsters from SARS CoV-2 variants by human polyclonal IgG from hyper-immunized transchromosomic bovines. Preprint at *bioRxiv* https://doi.org/10.1101/2021.07.26.453840 (2021).
16. McCray, P. B. Jr. et al. Lethal infection of K18-hACE2 mice infected with severe acute respiratory syndrome coronavirus. *J. Virol.* **81**, 813–821 (2007).
17. Winkler, E. S. et al. SARS-CoV-2 infection of human ACE2-transgenic mice causes severe lung inflammation and impaired function. *Nat. Immunol.* **21**, 1327–1335 (2020).
18. Armando, F. et al. SARS-CoV-2 Omicron variant causes mild pathology in the upper and lower respiratory tract of hamsters. *Nat. Commun.* **13**, 3519 (2022).
19. Meng, B. et al. Altered TMPRSS2 usage by SARS-CoV-2 Omicron impacts infectivity and fusogenicity. *Nature* **603**, 706–714 (2022).
20. Hoffmann, M. et al. SARS-CoV-2 cell entry depends on ACE2 and TMPRSS2 and is blocked by a clinically proven protease inhibitor. *Cell* **181**, 271–280.e8 (2020).
21. Jackson, C. B., Farzan, M., Chen, B. & Choe, H. Mechanisms of SARS-CoV-2 entry into cells. *Nat. Rev. Mol. Cell Biol.* **23**, 3–20 (2022).
22. Evans, J. P. & Liu, S. L. Role of host factors in SARS-CoV-2 entry. *J. Biol. Chem.* **297**, 100847 (2021).
23. Zhao, M. M. et al. Cathepsin L plays a key role in SARS-CoV-2 infection in humans and humanized mice and is a promising target for new drug development. *Signal Transduct. Target Ther.* **6**, 134 (2021).
24. Hui, K. P. Y. et al. SARS-CoV-2 Omicron variant replication in human bronchus and lung ex vivo. *Nature* **603**, 715–720 (2022).
25. Kimura, I. et al. Virological characteristics of the SARS-CoV-2 Omicron BA.2 subvariants, including BA.4 and BA.5 *Cell* **185**, 3992–4007.e16 (2022).
26. Davies, M.-A. et al. Outcomes of laboratory-confirmed SARS-CoV-2 infection during resurgence driven by Omicron lineages BA.4 and BA.5 compared with previous waves in the Western Cape Province, South Africa. Preprint at *medRxiv* https://doi.org/10.1101/2022.06.28.22276983 (2022).
27. Lewnard, J. A., Hong, V. & Tartof, S. Y. Association of SARS-CoV-2 BA.4/BA.5 Omicron lineages with immune escape and clinical outcome. Preprint at *medRxiv* https://doi.org/10.1101/2022.07.31.22278258 (2022).
28. Wolter, N. et al. Clinical severity of SARS-CoV-2 Omicron BA.4 and BA.5 lineages in South Africa. *Res. Sq.* https://doi.org/10.21203/rs.3.rs-1792132/v1 (2022).

Methods

Cells

VeroE6/TMPRSS2 (JCRB 1819) cells[29] were propagated in the presence of 1 mg ml^{-1} geneticin (G418; Invivogen) and 5 μg ml^{-1} plasmocin prophylactic (Invivogen) in Dulbecco's modified Eagle's medium containing 10% fetal calf serum. VeroE6-TMPRSS2-T2A-ACE2 cells (provided by B. Graham, NIAID Vaccine Research Centre) were cultured in Dulbecco's modified Eagle's medium supplemented with 10% fetal calf serum, 10 mM HEPES pH 7.3, 100 U ml^{-1} of penicillin–streptomycin and 10 μg ml^{-1} puromycin. VeroE6/TMPRSS2 and VeroE6-TMPRSS2-T2A-ACE2 cells were maintained at 37 °C with 5% CO_2. The cells were regularly tested for mycoplasma contamination by using PCR and confirmed to be mycoplasma-free.

Viruses

hCoV-19/Japan/UT-NCD1288-2N/2022 (BA.2; NCD1288)[4,30], hCoV-19/Japan/TY41-703/2022 (BA.4; TY41-703), hCoV-19/Japan/TY41-702/2022 (BA.5; TY41-702), hCoV-19/Japan/TY41-704/2022 (BA.5; TY41-704) and hCoV-19/USA/WI-UW-5250/2021 (B.1.617.2; UW5250)[1,31] were propagated in VeroE6/TMPRSS2 cells in VP-SFM (Thermo Fisher Scientific). hCoV-19/USA/MD/HP30386/2022 (BA.4; HP30386) and SARS-CoV-2/human/USA/COR-22-063113/2022 (BA.5; COR-22-063113) were propagated in VeroE6-TMPRSS2-T2A-ACE2 cells in VP-SFM (Thermo Fisher Scientific). TY41-703 (BA.4), COR-22-063113 (BA.5) and TY41-704 (BA.5) were subjected to NGS (see Whole-genome sequencing); amino acid differences between these viruses and the reference sequence (Wuhan/Hu-1/2019) are shown in Extended Data Table 1. All experiments with SARS-CoV-2 were performed in enhanced biosafety level 3 containment laboratories at the University of Tokyo and the National Institute of Infectious Diseases, Japan, which are approved for such use by the Ministry of Agriculture, Forestry, and Fisheries, Japan, or in biosafety level 3 agriculture containment laboratories at the University of Wisconsin, Madison, which are approved for such use by the Centers for Disease Control and Prevention and by the US Department of Agriculture.

Animal experiments and approvals

Animal studies were carried out in accordance with the recommendations in the Guide for the Care and Use of Laboratory Animals of the National Institutes of Health. The protocols were approved by the Animal Experiment Committee of the Institute of Medical Science, the University of Tokyo (approval number PA19-75) and the Institutional Animal Care and Use Committee at the University of Wisconsin, Madison (assurance number V006426). Virus inoculations were performed under isoflurane, and all efforts were made to minimize animal suffering. In vivo studies were not blinded, and animals were randomly assigned to infection groups. No sample-size calculations were performed to power each study. Instead, sample sizes were determined based on previous in vivo virus challenge experiments.

Experimental infection of Syrian hamsters

Six-week-old male wild-type Syrian hamsters (Japan SLC Inc.) were used in this study. Baseline body weights were measured before infection. Under isoflurane anaesthesia, five hamsters per group were intranasally inoculated with 10^5 PFU (in 30 μl) of BA.2 (NCD1288), BA.4 (HP30386 or TY41-703), BA.5 (COR-22-063113, TY41-702 or TY41-704) or B.1.617.2 (UW5250). Body weight was monitored daily for 10 days. For virological and pathological examinations, ten hamsters per group were intranasally infected with 10^5 PFU (in 30 μl) of BA.2 (NCD1288), BA.4 (HP30386), BA.5 (COR-22-063113) or B.1.617.2 (UW5250); 3 and 6 dpi, five animals were euthanized and nasal turbinates and lungs were collected. The virus titres in the nasal turbinates and lungs were determined by use of plaque assays on VeroE6-TMPRSS2-T2A-ACE2 cells.

The K18-hACE2 transgenic hamster lines (line M41) were developed by using a piggyBac-mediated transgenic approach. The K18-hACE2 cassette from the pK18-hACE2 plasmid was transferred into a piggyBac vector, pmhyGENIE-3[32], for pronuclear injection[15]. Then, 5- to 10-week-old K18-hACE2 homozygous transgenic hamsters, for which hACE2 expression was confirmed, were intranasally inoculated with 10^5 PFU (in 30 μl) of BA.2(NCD1288) (gender: two males and two females), BA.4 (HP30386) (gender: one male and three females), BA.5 (COR-22-063113) (gender: one male and three females) or B.1.617.2 (UW5250) (gender: two males and two females). Body weight was monitored daily for 5 days. At 5 dpi, the animals were euthanized and nasal turbinates and lungs were collected. The virus titres in the nasal turbinates and lungs were determined by use of plaque assays on VeroE6-TMPRSS2-T2A-ACE2 cells.

For co-infection studies in wild-type hamsters, BA.2 (NCD1288) was mixed with BA.4 (HP30386) or BA.5 (COR-22-063113) at an equal ratio on the basis of their titre, and the virus mixture (total 2×10^5 PFU in 60 μl) was inoculated into ten wild-type hamsters. At 2 and 4 dpi, five animals were euthanized and nasal turbinates and lungs were collected. For co-infection studies in K18-hACE2 transgenic female hamsters, BA.2 (NCD1288) was mixed with BA.5 (COR-22-063113) at a 1:1 or 3:1 ratio on the basis of their titre, and each virus mixture (total 2×10^5 PFU in 60 μl) was inoculated into five K18-hACE2 transgenic hamsters. At 3 dpi, all five animals were euthanized and nasal turbinates and lungs were collected.

Experimental infection of K18-hACE2 mice

Ten-week-old female K18-hACE2 mice (Jackson Laboratory) were used in this study. Baseline body weights were measured before infection. Under isoflurane anaesthesia, five mice per group were intranasally inoculated with 10^5 PFU (in 25 μl) of BA.2 (NCD1288), BA.4 (HP30386), BA.5 (COR-22-063113) or B.1.617.2 (UW5250). Body weight was monitored daily for 10 days. For virological examination, five mice per group were intranasally infected with 10^5 PFU (in 25 μl) of BA.2 (NCD1288), BA.4 (HP30386), BA.5 (COR-22-063113), BA.5 (TY41-702) or B.1.617.2 (UW5250); 2 and 5 dpi, five animals were euthanized and lungs were collected. The virus titres in the lungs were determined by use of plaque assays on VeroE6-TMPRSS2-T2A-ACE2 cells.

Lung function

Respiratory parameters were measured by using a whole-body plethysmography system (PrimeBioscience) according to the manufacturer's instructions. In brief, infected hamsters were placed in the unrestrained plethysmography chambers and allowed to acclimatize for 1 min before data were acquired over a 3 min period by using FinePointe software.

Histopathology

Histopathological examination was performed as previously described[1,4]. In brief, excised animal lungs were fixed in 4% paraformaldehyde in phosphate-buffered saline and processed for paraffin embedding. The paraffin blocks were sliced into 3 μm thick sections and mounted on silane-coated glass slides, followed by haematoxylin and eosin stain for histopathological examination. Tissue sections were also processed for immunohistochemistry with a rabbit polyclonal antibody for SARS-CoV nucleocapsid protein (ProSpec; ANT-180, 1:500 dilution, Rehovot, Israel), which cross-reacts with SARS-CoV-2 nucleocapsid protein. Specific antigen–antibody reactions were visualized by staining with 3,3'-diaminobenzidine tetrahydrochloride and by using the Dako Envision system (Dako Cytomation; K4001, 1:1 dilution, Glostrup, Denmark). To detect SARS-CoV-2 RNA, in situ hybridization was performed by using an RNA scope 2.5 HD Red Detection kit (Advanced Cell Diagnostics, Newark, California) with an antisense probe targeting the nucleocapsid gene of SARS-CoV-2 (Advanced Cell Diagnostics) and following the manufacturer's instructions.

Histopathological scores of inflammation in the alveolar regions were determined based on the percentage of alveolar inflammation in a given area of a pulmonary section collected from each animal in each group by using the following scoring system: 0, no inflammation; 1, affected

area (≤1%); 2, affected area (>1%, ≤10%); 3, affected area (>10%, ≤50%); 4, affected area (>50%). An additional point was added when pulmonary oedema and/or alveolar haemorrhage was observed. Therefore, histopathological scores of inflammation in the alveoli for individual animals ranged from 0 to 5. Immunohistochemistry scores were determined based on the percentage of viral antigen-positive cells, detected by immunohistochemistry, in a high-power field by using the following scoring system: 0, no positive cells; 1, positive cells (≤10%); 2, positive cells (>10%, ≤25%); 3, positive cells (>25%, ≤50%); 4, positive cells (>50%). Immunohistochemistry scores for each animal were calculated for bronchial/bronchiolar and alveolar regions, respectively, as a total score for the three high-power fields with the highest positivity rate on the section; the scores for individual animals ranged from 0 to 12.

Whole-genome sequencing

Viral RNA was extracted by using a QIAamp Viral RNA Mini Kit (QIAGEN). The whole genome of SARS-CoV-2 was amplified by using a modified ARTIC network protocol in which some primers were replaced or added[33,34]. In brief, viral complementary deoxoribonucleic acid was synthesized from the extracted RNA by using a LunarScript RT SuperMix Kit (New England BioLabs). The DNA was then amplified by performing a multiplexed PCR in two pools by using the ARTIC-N5 primers[35] and the Q5 Hot Start DNA polymerase (New England BioLabs). The DNA libraries for Illumina NGS were prepared from pooled amplicons by using a QIAseq FX DNA Library Kit (QIAGEN) and were then analysed by using the iSeq 100 System (Illumina). To determine the sequence of TY41-703 (BA.4), COR-22-063113 (BA.5) and TY41-704 (BA.5), the reads were assembled by the CLC Genomics Workbench (v.22, Qiagen) with the Wuhan/Hu-1/2019 sequence (GenBank accession no. MN908947) as a reference. The sequences of TY41-703 (BA.4), COR-22-063113 (BA.5) and TY41-704 (BA.5) were deposited in the Genbank with accession IDs OP603964, OP603961 and OP603965, respectively. For the analysis of the ratio of BA.2 to BA.4 or BA.5 after co-infection, the ratio of BA.2 to BA.4 or BA.5 was calculated from the 5 amino acid differences in the S gene between the two viruses. Samples with more than 300 read-depths were analysed.

Statistical analysis

GraphPad Prism software was used to analyse all of the data. Statistical analysis included the Kruskal–Wallis test followed by Dunn's test and ANOVA with post-hoc tests. Differences among groups were considered significant for P values less than 0.05.

Reporting summary

Further information on research design is available in the Nature Portfolio Reporting Summary linked to this article.

Data availability

All data supporting the findings of this study are available in the paper. There are no restrictions in obtaining access to the primary data. Source data are provided with this paper. The sequences of the viruses (BA.4 [TY41-703], BA.5 [COR-22-063113] and BA.5 [TY41-704]) were deposited in the Genbank with accession IDs OP603964, OP603961 and OP603965, respectively.

Code availability

No code was used in the course of the data acquisition or analysis.

29. Matsuyama, S. et al. Enhanced isolation of SARS-CoV-2 by TMPRSS2-expressing cells. *Proc. Natl Acad. Sci. USA* **117**, 7001–7003 (2020).
30. Takashita, E. et al. Efficacy of antiviral agents against the SARS-CoV-2 Omicron subvariant BA.2. *N. Engl. J. Med.* **386**, 1475–1477 (2022).
31. Gagne, M. et al. Protection from SARS-CoV-2 delta one year after mRNA-1273 vaccination in rhesus macaques coincides with anamnestic antibody response in the lung. *Cell* **185**, 113–130.e15 (2022).
32. Li, Z. et al. Generation of transgenic pigs by cytoplasmic injection of piggyBac transposase-based pmGENIE-3 plasmids. *Biol. Reprod.* **90**, 93 (2014).
33. Quick, J. nCoV-2019 sequencing protocol. *Protocol.io* https://www.protocols.io/view/ncov-2019-sequencing-protocol-v3-locost-bh42j8ye?version_warning=no (2020).
34. Itokawa, K., Sekizuka, T., Hashino, M., Tanaka, R. & Kuroda, M. Disentangling primer interactions improves SARS-CoV-2 genome sequencing by multiplex tiling PCR. *PLoS ONE* **15**, e0239403 (2020).
35. Itokawa, K. et al. nCoV-2019 sequencing protocol for illumina V.5. *Protocol.io* https://www.protocols.io/view/ncov-2019-sequencing-protocol-for-illumina-b2msqc6e?version_warning=no (2021).

Acknowledgements We thank S. Watson for scientific editing. We also thank K. Yokota, N. Mizutani, K. Kajiyama, Y. Sato and S. Ozono for technical assistance. VeroE6-TMPRSS2-T2A-ACE2 cells were provided by B. Graham, NIAID Vaccine Research Center. This work was supported by a Research Programme on Emerging and Re-emerging Infectious Diseases (grant nos. JP21fk0108552 and JP22fk0108637), a Project Promoting Support for Drug Discovery (grant no. JP20nk0101632), the Japan Programme for Infectious Diseases Research and Infrastructure (grant no. JP22wm0125002), a grant (grant no. JP223fa627001) from the Japan Agency for Medical Research and Development, the National Institutes of Allergy and Infectious Diseases Center for Research on Influenza Pathogenesis (grant no. HHSN272201400008C) and the Center for Research on Influenza Pathogenesis and Transmission (grant no. 75N93021C00014).

Author contributions R.U., P.J.H., S.I., S.Y., Y.F., M. Kiso, M. Ito, K.I.-H., S.M., M. Kuroda, T.M., H.U., M. Imai and T.S. performed the hamster infection experiments, titrated the virus in tissues and analysed the pathology. S.Y. performed the NGS. Z.W., R.L., Y.L. and D.L. generated the hACE2 hamsters. S.Y., Y.S.-T., S.F., S.W., K.M., A.P., A.K. and R.J.W. propagated and/or sequenced the viruses. R.U., P.J.H., S.I., S.Y., M. Imai, T.S. and Y.K. obtained funding, conceived the study and/or supervised the research. R.U., Y.F., M. Imai and Y.K. wrote the initial draft, with all other authors providing editorial comments.

Competing interests Y.K. has received unrelated funding support from Daiichi Sankyo Pharmaceutical, Toyama Chemical, Tauns Laboratories, Inc., Shionogi & Co. LTD, Otsuka Pharmaceutical, KM Biologics, Kyoritsu Seiyaku, Shinya Corporation and Fuji Rebio. The remaining authors declare no competing interests.

Additional information

Supplementary information The online version contains supplementary material available at https://doi.org/10.1038/s41586-022-05482-7.

Correspondence and requests for materials should be addressed to Masaki Imai, Tadaki Suzuki or Yoshihiro Kawaoka.

Peer review information *Nature* thanks Charaf Benarafa and the other, anonymous, reviewer(s) for their contribution to the peer review of this work.

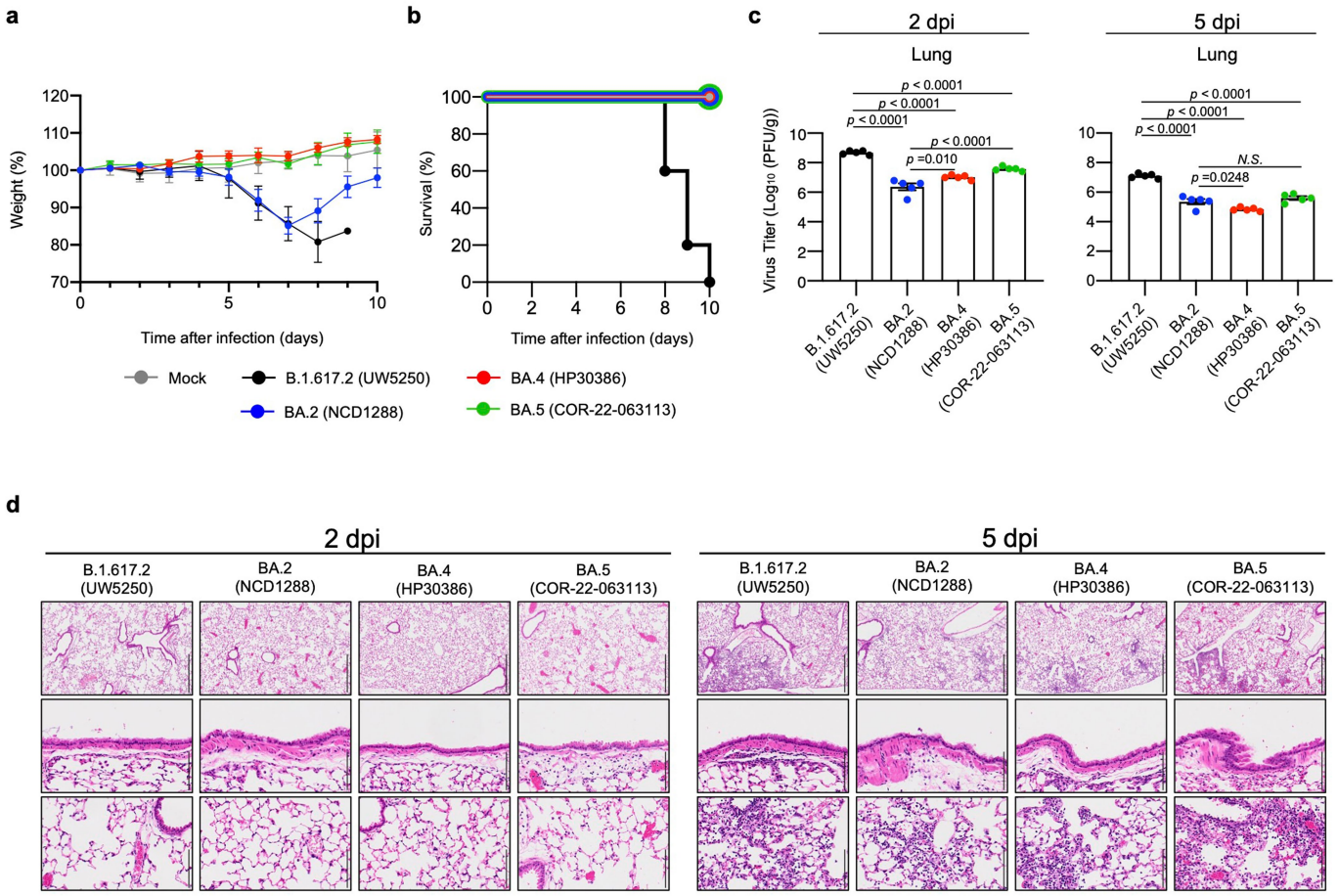

Extended Data Fig. 1 | The replication and pathogenicity of BA.4 and BA.5 in K18-hACE2 mice. a–**c**, K18-hACE2 mice ($n = 5$) were intranasally inoculated with 10^5 PFU in 25 µL of BA.2 (NCD1288), BA.4 (HP30386), BA.5 (COR-22-063113), B.1.617.2 (UW5250) or PBS. Body weights (**a**) and survival (**b**) were monitored daily for 10 days. The data are presented as the mean percentages of the starting weight ± SEM. **c**, Infected mice were euthanized at 2 and 5 dpi for virus titration ($n = 5$ group^{-1}). Virus titre in the lungs were determined by performing plaque assays with Vero E6-TMPRSS2-T2A-ACE2 cells. Vertical bars show the mean ± SEM. Points indicate data from individual mice. The lower limit of detection is indicated by the horizontal dashed line. Data were analysed by using a one-way ANOVA with Tukey's multiple comparisons test (titre at 2 dpi and 5 dpi). *P* values of less than 0.05 were considered statistically significant. **d**, Infected mice were euthanized at 2 and 5 dpi for histopathological examinations. Representative images of the lungs are shown. Upper rows, the lungs at low magnification. Middle rows, bronchial/bronchiolar regions. Lower rows, alveolar regions. Scale bars: 500 µm in the upper rows, 100 µm in the middle and lower rows. Data are from one experiment.

Extended Data Table 1 | Amino acid mutations in the clinical isolates of BA.2, BA.4 and BA.5 used in this study

Protein			Position	Virus (Pango lineage)						
				Early SARS-CoV-2 (A)	hCoV-19/Japan/UT-NCD1288-2N-2022 (BA.2)	hCoV-19/USA/MD/HP30386/2022 (BA.4)	hCoV-19/Japan/TY41-703/2022 (BA.4)	SARS-CoV-2/human/USA/COR-22-063113/2022 (BA.5)	hCoV-19/Japan/TY41-702/2022 (BA.5)	hCoV-19/Japan/TY41-704/2022 (BA.5)
ORF1a			135	Ser	Arg	Arg	Arg	Arg	Arg	Arg
			141	Lys	Lys	del[a]	del	Lys	Lys	Lys
			142	Gly	Gly	del	del	Gly	Gly	Gly
			143	Phe	Phe	del	del	Phe	Phe	Phe
			556	Gln	Gln	Gln	Gln	Gln	Lys	Gln
			842	Thr	Ile	Ile	Ile	Ile	Ile	Ile
			1307	Gly	Ser	Ser	Ser	Ser	Ser	Ser
			2139	Ala	Ala	Ala	Thr	Ala	Ala	Ala
			2153	Thr	Thr	Ile	Thr	Thr	Thr	Thr
			2648	Thr	Thr	Thr	Thr	Thr	Thr	Ile
			3027	Leu	Phe	Phe	Phe	Phe	Phe	Phe
			3090	Thr	Ile	Ile	Ile	Ile	Ile	Ile
			3201	Leu	Phe	Leu	Leu	Leu	Leu	Leu
			3255	Thr	Ile	Ile	Ile	Ile	Ile	Ile
			3395	Pro	His	His	His	His	His	His
			3515	Pro	Pro	Pro	Pro	Leu (62%)	Pro	Pro
			3557	Phe	Phe	Phe	Phe	Phe	Phe	Leu
			3650	Phe	Phe	Phe	Phe	Phe	Leu (85%)	Phe
			3675	Ser	del	del	del	del	del	del
			3676	Gly	del	del	del	del	del	del
			3677	Phe	del	del	del	del	del	del
			3753	Phe	Val(20%)	Phe	Phe	Phe	Phe	Phe
			3829	Leu	Leu	Leu	Phe (71%)	Phe (33%)	Leu	Leu
			4159	Thr	Thr	Ile	Thr	Thr	Thr	Thr
			4391	Leu	Phe(19%)	Leu	Leu	Leu	Leu	Leu
ORF1b			314	Pro	Leu	Leu	Leu	Leu	Leu	Leu
			662	Gly	Val	Gly	Gly	Gly	Gly	Gly
			959	Ser	Pro	Ser	Ser	Ser	Ser	Ser
			1156	Met	Met	Met	Met	Met	Ile	Met
			1161	Pro	Ser(27%)	Pro	Pro	Pro	Pro	Pro
			1315	Arg	Cys	Cys	Cys	Cys	Cys	Cys
			1566	Ile	Val	Val	Val	Val	Val	Val
			2163	Thr	Ile	Ile	Ile	Ile	Ile	Ile
			2497	Leu	Leu	Phe (73%)	Leu	Leu	Leu	Leu
			2513	Ala	Val(18%)	Ala	Ala	Ala	Ala	Ala
S	S1 (1-684)	SP (1-12)	3	Val	Val	**Gly**	**Gly**	Val	Val	Val
		NTD (13-304)	19	Thr	Ile	Ile	Ile	Ile	Ile	Ile
			24	Leu	del	del	del	del	del	del
			25	Pro	del	del	del	del	del	del
			26	Pro	del	del	del	del	del	del
			27	Ala	Ser	Ser	Ser	Ser	Ser	Ser
			69	His	His	**del**	**del**	**del**	**del**	**del**
			70	Val	Val	**del**	**del**	**del**	**del**	**del**
			76	Thr	Thr	Thr	Thr	**Ile**	Thr	Thr
			142	Gly	Asp	Asp	Asp	Asp	Asp	Asp
			213	Val	Gly	Gly	Gly	Gly	Gly	Gly
		RBD (331-527)	339	Gly	Asp	Asp	Asp	Asp	Asp	Asp
			371	Ser	Phe	Phe	Phe	Phe	Phe	Phe
			373	Ser	Pro	Pro	Pro	Pro	Pro	Pro
			375	Ser	Phe	Phe	Phe	Phe	Phe	Phe
			376	Thr	Ala	Ala	Ala	Ala	Ala	Ala
			405	Asp	Asn	Asn	Asn	Asn	Asn	Asn
			408	Arg	Ser	Ser	Ser	Ser	Ser	Ser
			417	Lys	Asn	Asn	Asn	Asn	Asn	Asn
			440	Asn	Lys	Lys	Lys	Lys	Lys	Lys
			452	Leu	Leu	**Arg**	**Arg**	**Arg**	**Arg**	**Arg**
			477	Ser	Asn	Asn	Asn	Asn	Asn	Asn
			478	Thr	Lys	Lys	Lys	Lys	Lys	Lys
			484	Glu	Ala	Ala	Ala	Ala	Ala	Ala
			486	Phe	Phe	**Val**	**Val**	**Val**	**Val**	**Val**
			493	Gln	Arg	**Gln**	**Gln**	**Gln**	**Gln**	**Gln**
			498	Gln	Arg	Arg	Arg	Arg	Arg	Arg
			501	Asn	Tyr	Tyr	Tyr	Tyr	Tyr	Tyr
			505	Tyr	His	His	His	His	His	His
		SD1/2 (528-684)	614	Asp	Gly	Gly	Gly	Gly	Gly	Gly
			655	His	Tyr	Tyr	Tyr	Tyr	Tyr	Tyr
			679	Asn	Lys	Lys	Lys	Lys	Lys	Lys
			681	Pro	His	His	His	His	His	His
			682	Arg	Arg	Arg	Arg	Arg	Arg	**Trp (10%)**
	S2 (685-1210)		764	Asn	Lys	Lys	Lys	Lys	Lys	Lys
			796	Asp	Tyr	Tyr	Tyr	Tyr	Tyr	Tyr
			954	Gln	His	His	His	His	His	His
			969	Asn	Lys	Lys	Lys	Lys	Lys	Lys
ORF3a			223	Thr	Ile	Ile	Ile	Ile	Ile	Ile
E			9	Thr	Ile	Ile	Ile	Ile	Ile	Ile
			14	Val	Val	del (57%)	Val	del (48%)	Val	Val
M			3	Asp	Asp	Asp	Asp	Asn	Asn	Asp
			19	Gln	Glu	Glu	Glu	Glu	Glu	Glu
			63	Ala	Thr	Thr	Thr	Thr	Thr	Thr
			131	Arg	Arg	Arg	Arg	Arg	Arg	Thr
ORF6			57	Pro	Pro	Pro	Pro	Pro	Pro	Leu
			61	Asp	Leu	Leu	Leu	Asp	Asp	Asp
ORF7b			10	Pro	Ser	Pro	Pro	Pro	Pro	Pro
			11	Leu	Leu	Phe	Phe	Leu	Leu	Leu
			27	Glu	del	Glu	Glu	Glu	Glu	Glu
			28	Asn	del	Asn	Asn	Asn	Asn	Asn
			29	Ala	del	Ala	Ala	Ala	Ala	Ala
N			13	Pro	Leu	Leu	Leu	Leu	Leu	Leu
			31	Glu	del	del	del	del	del	del
			32	Arg	del	del	del	del	del	del
			33	Ser	del	del	del	del	del	del
			136	Glu	Glu	Glu	Glu	Glu	Asp	Glu
			151	Pro	Pro	Ser	Ser	Pro	Pro	Pro
			203	Arg	Lys	Lys	Lys	Lys	Lys	Lys
			204	Gly	Arg	Arg	Arg	Arg	Arg	Arg
			413	Ser	Arg	Arg	Arg	Arg	Arg	Arg
ORF10			29	Gln	Gln	Gln	Stop (22%)	Gln	Gln	Gln

Compared with the reference strain Wuhan/Hu-1/2019, mutations are shown. The spike protein is composed of two subunits, S1 and S2. Compared with BA.2 (hCoV-19/Japan/UT-NCD1288-2N/2022), spike protein mutations are shown in bold red for BA.4 and in blod blue for BA.5. ORF, open reading frame; SP, signal peptide; NTD, N-terminal domain; RBD, receptor-binding domain; SD1/2, subdomain 1 and 2; E, Envelope; M, Membrane; and N, Nucleocapsid.del[a]; deletion.

nature portfolio

Corresponding author(s): Yoshihiro Kawaoka

Last updated by author(s): Oct 11, 2022

Reporting Summary

Nature Portfolio wishes to improve the reproducibility of the work that we publish. This form provides structure for consistency and transparency in reporting. For further information on Nature Portfolio policies, see our Editorial Policies and the Editorial Policy Checklist.

Statistics

For all statistical analyses, confirm that the following items are present in the figure legend, table legend, main text, or Methods section.

n/a	Confirmed	
☐	☒	The exact sample size (*n*) for each experimental group/condition, given as a discrete number and unit of measurement
☐	☒	A statement on whether measurements were taken from distinct samples or whether the same sample was measured repeatedly
☐	☒	The statistical test(s) used AND whether they are one- or two-sided *Only common tests should be described solely by name; describe more complex techniques in the Methods section.*
☒	☐	A description of all covariates tested
☐	☒	A description of any assumptions or corrections, such as tests of normality and adjustment for multiple comparisons
☐	☒	A full description of the statistical parameters including central tendency (e.g. means) or other basic estimates (e.g. regression coefficient) AND variation (e.g. standard deviation) or associated estimates of uncertainty (e.g. confidence intervals)
☐	☒	For null hypothesis testing, the test statistic (e.g. *F*, *t*, *r*) with confidence intervals, effect sizes, degrees of freedom and *P* value noted *Give P values as exact values whenever suitable.*
☒	☐	For Bayesian analysis, information on the choice of priors and Markov chain Monte Carlo settings
☒	☐	For hierarchical and complex designs, identification of the appropriate level for tests and full reporting of outcomes
☒	☐	Estimates of effect sizes (e.g. Cohen's *d*, Pearson's *r*), indicating how they were calculated

Our web collection on statistics for biologists contains articles on many of the points above.

Software and code

Policy information about availability of computer code

Data collection	iSeq 100 System (Illumina) FinePointe software version 2.8.0.12146(SATRR)
Data analysis	Prism 8.0 was used for the statistical analysis. The NGS reads were assembled by the CLC Genomics Workbench (version 22, Qiagen).

For manuscripts utilizing custom algorithms or software that are central to the research but not yet described in published literature, software must be made available to editors and reviewers. We strongly encourage code deposition in a community repository (e.g. GitHub). See the Nature Portfolio guidelines for submitting code & software for further information.

Data

Policy information about availability of data

All manuscripts must include a data availability statement. This statement should provide the following information, where applicable:

- Accession codes, unique identifiers, or web links for publicly available datasets
- A description of any restrictions on data availability
- For clinical datasets or third party data, please ensure that the statement adheres to our policy

All data supporting the findings of this study are available in the paper. There are no restrictions in obtaining access to the primary data. The source data are provided with this paper. The sequences of the viruses [BA.4 (TY41-703), BA.5 (COR-22-063113), and BA.5 (TY41-704)] were deposited in the Genbank with Accession IDs: OP603964, OP603961, and OP603965, respectively.

Field-specific reporting

Please select the one below that is the best fit for your research. If you are not sure, read the appropriate sections before making your selection.

☒ Life sciences ☐ Behavioural & social sciences ☐ Ecological, evolutionary & environmental sciences

For a reference copy of the document with all sections, see nature.com/documents/nr-reporting-summary-flat.pdf

Life sciences study design

All studies must disclose on these points even when the disclosure is negative.

Sample size	No sample-size calculations were performed. No statistical method was used to determine sample size. Wild-type hamster, hACE2-expressing hamster, and hACE2-expressing mouse experiments were performed with at least n = 5, n = 3 and n = 5, respectively, per group. All sample sizes were chosen based on prior experience (PMID: 34846168, 34668780, 32839612, 34140350, and 32571934).
Data exclusions	No data exclusions.
Replication	All experiments with multiple biological replicates are indicated in the figure legends.
Randomization	No method of randomization was used to determine how the animals were allocated to the experimental groups and processed in this study. However, covariates including sex and age were identical in groups.
Blinding	No blinding was carried out due to the limited number of staff available to conduct these studies.

Reporting for specific materials, systems and methods

We require information from authors about some types of materials, experimental systems and methods used in many studies. Here, indicate whether each material, system or method listed is relevant to your study. If you are not sure if a list item applies to your research, read the appropriate section before selecting a response.

Materials & experimental systems

n/a	Involved in the study
☐	☒ Antibodies
☐	☒ Eukaryotic cell lines
☒	☐ Palaeontology and archaeology
☐	☒ Animals and other organisms
☒	☐ Human research participants
☒	☐ Clinical data
☒	☐ Dual use research of concern

Methods

n/a	Involved in the study
☒	☐ ChIP-seq
☒	☐ Flow cytometry
☒	☐ MRI-based neuroimaging

Antibodies

Antibodies used	A rabbit polyclonal antibody for SARS-CoV nucleocapsid protein (ProSpec; ANT-180, 1:500 dilution, Rehovot, Israel) was used for immunohistochemical staining.
Validation	The rabbit polyclonal antibody for SARS-CoV nucleocapsid protein (ProSpec; ANT-180, Rehovot, Israel) was validated in previous publications: Imai, M. et al. Syrian hamsters as a small animal model for SARS-CoV-2 infection and countermeasure development. Proc Natl Acad Sci U S A 117, 16587-16595, doi:10.1073/pnas.2009799117 (2020); Imai, M. et al. Characterization of a new SARS-CoV-2 variant that emerged in Brazil. Proc Natl Acad Sci U S A 118, doi:10.1073/pnas.2106535118 (2021); Halfmann, P. J. et al. SARS-CoV-2 Omicron virus causes attenuated disease in mice and hamsters. Nature, doi:10.1038/s41586-022-04441-6 (2022).

Eukaryotic cell lines

Policy information about cell lines

Cell line source(s)	VeroE6/TMPRSS2 cells (available at Japanese Collection of Research Bioresources Cell Bank, JCRB 1819), Vero E6-TMPRSS2-T2A-ACE2 cells, VRC/NIH (available at BEi Resources, NR-54970).
Authentication	Vero/TMPRSS2 and Vero E6-TMPRSS2-T2A-ACE2 cells were assumed to be authentic by the cell bank or manufactures. No further authentication was performed by the authors.
Mycoplasma contamination	All cell lines are routinely tested each month and were negative for mycoplasma.

Commonly misidentified lines (See ICLAC register)	No commonly misidentified lines were used in this study.

Animals and other organisms

Policy information about studies involving animals; ARRIVE guidelines recommended for reporting animal research

Laboratory animals	Heterozygous female K18-hACE2 C57BL/6J mice (strain 2B6.Cg-Tg(K18-ACE2)2Prlmn/J, 10-week-old) were obtained from the Jackson Laboratory. Male Syrian hamsters (6-week-old) were obtained from Japan SLC Inc., Shizuoka, Japan. The K18-hACE2 transgenic female hamsters (lineM41; mixed gender, 5- to 10-week-old) are described in detail elsewhere (lines M41; Gilliland T. et al. bioRxiv, doi:10.1101/2021.07.26.453840).
Wild animals	No wild animals were used in this study.
Field-collected samples	This study did not involve samples collected from the field.
Ethics oversight	Animal studies were carried out in accordance with the recommendations in the Guide for the Care and Use of Laboratory Animals of the National Institutes of Health. The protocols were approved by the Institutional Animal Care and Use Committee at University of Wisconsin, Madison (V006426) and the Animal Experiment Committee of the Institute of Medical Science, the University of Tokyo (approval number PA19-75).

Note that full information on the approval of the study protocol must also be provided in the manuscript.